CONF-861207--91

COMBINED ATOM-PROBE AND ELECTRON MICROSCOPY CHARACTERIZATION OF FINE SCALE STRUCTURES IN AGED PRIMARY COOLANT PIPE STAINLESS STEEL

CONF-861207--91

DE87 007365

J. BENTLEY AND M. K. MILLER

Metals and Ceramics Division,
Building 5500, MS-376
Oak Ridge National Laboratory,
Oak Ridge, TN 37831-6376.

To be published in the Proceedings of the Materials Research Society Meeting, Dec. 1-5, 1986, Boston.

DISCLAIMER

COMBINED ATOM-PROBE AND ELECTRON MICROSCOPY CHARACTERIZATION OF FINE SCALE STRUCTURES IN AGED PRIMARY COOLANT PIPE STAINLESS STEEL

J. BENTLEY AND M. K. MILLER
Metals and Ceramics Division, Oak Ridge National Laboratory, Oak Ridge, TN 37831.

ABSTRACT

The capabilities and complementary nature of atom probe field-ion microscopy (APFIM) and analytical electron microscopy (AEM) for the characterization of fine-scale microstructures are illustrated by examination of the changes that occur after long term thermal aging of cast CF 8 and CF 8M duplex stainless steels. In material aged at 300 or 400°C for up to 70,000 h, the ferrite had spinodally decomposed into a modulated fine-scaled interconnected network consisting of an iron-rich α phase and a chromium-enriched α' phase with periodicities of between 2 and 9 nm. G-phase precipitates 2 to 10 nm in diameter were also observed in the ferrite at concentrations of more than 10^{21} m^{-3}. The reported degradation in mechanical properties is most likely a consequence of the spinodal decomposition in the ferrite.

INTRODUCTION

In order to make structure-property correlations, high quality, comprehensive microstructural analysis is required. Mechanical properties are often determined by nanometer scale microstructural features such as secondary defect clusters or precipitates. This work shows how atom-probe field-ion microscopy (APFIM) and analytical electron microscopy (AEM) form an extremely powerful combination for such microstructural analysis.

The aims of this paper are to illustrate the advantages and limitations of each technique for the characterization of fine scale structures, to present the complementary nature of the techniques and, thirdly, to explain the degradation of mechanical properties observed after long-term thermal aging of primary coolant pipe stainless steel. A general knowledge of APFIM and AEM will be assumed[1,2] but the characteristics relevant to the specific application will be described.

The mechanical properties of CF 8 and CF 8M cast stainless steels used for the primary coolant pipes in pressurized light-water nuclear reactors (service temperature about 300°C) may be degraded by extended aging at 300 to 400°C. Of particular concern is the dramatic loss in impact properties to approximately 15% of the initial value[3]. The cast steels have a duplex microstructure consisting of austenite (γ) with 15 to 20% δ-ferrite. The ferrite increases the yield strength and reduces the susceptibility to hot cracking. During aging, the ferrite decomposes spinodally into a fine scaled interconnected network of iron-rich α phase and chromium-enriched α' phase[4-7]. In addition, fine particles of G-phase, a complex silicide, are formed[4-7]. These fine scale phase transformations are believed to be responsible for the degradation of mechanical properties.

EXPERIMENTAL

The compositions of the CF 8 and CF 8M steels used in this investigation are given in Table 1. The CF 8 steel was examined after laboratory aging for 70,000 h at 300 or 400°C. The CF 8M steel was examined in both the as-cast condition and also after aging for 7,500 h at 400°C. The APFIM analyses were conducted on the ORNL[8] and Oxford atom probes. The AEM analyses were performed with Philips EM400T/FEG and EM430T analytical electron microscopes both equipped with 6585 STEM units, EDAX 9100/70 energy dispersive X-ray spectrometers (EDS), and Gatan 607 electron energy loss spectrometer (EELS) systems. A standardless procedure was used to obtain elemental compositions from EDS data[9].

Table 1. Nominal compositions of the CF 8 and CF 8M steels (wt.%)

Alloy	Cr	Ni	Si	Mn	Mo	C	N	S	P	Fe
CF 8	20.2	8.3	1.0	0.28	0.13	0.038	0.027	0.019	0.008	Balance
CF 8M	20.8	10.6	0.81	0.79	2.5	0.04	0.042	0.021	0.016	Balance

MICROSTRUCTURAL CHARACTERIZATION

Transmission electron microscopy (TEM) confirmed the general microstructural features observed by optical microscopy, i.e. the duplex nature of the steel with about 15% ferrite. Only the expected medium density of dislocations was observed in the austenite with no precipitation evident. A low density of dislocations was observed in the ferrite accompanied by a fine distribution of G-phase precipitates (see below). The γ-δ interface structure was also characterized. These boundaries in the CF 8 aged at 300°C and in the CF 8M, were largely free of precipitates. However, in the CF 8 aged at 400°C, a reverted layer was observed with extensive precipitation of $M_{23}C_6$ particles [Fig. 1(a)] oriented cube-on-cube with the γ. Compositions of the phases determined by EDS are given in Table 2. The Cr contents of the austenite and ferrite are probably overestimated by up to 2 at.% Cr since no corrections for fluorescence effects were made. EELS analyses of the $M_{23}C_6$ particles confirmed the presence of carbon.

APFIM examination of the austenite also revealed no fine scale precipitation had occurred after aging, whereas the ferrite was found to have undergone marked changes in microstructure and microchemistry. In the aged CF 8M, numerous ($10^{23}m^{-3}$), 10 nm in diameter roughly spherical, brightly imaging, precipitates were observed [Fig. 1(b)]. APFIM selected area microchemical analyses of the central portion of five precipitates in the aged CF 8M steel revealed that they were complex alloy silicides (Table 3). Composition profiles made between the precipitates clearly indicated decomposition into iron-rich and chromium-enriched regions on a scale of ~2 nm had occurred (Fig 2). These changes in the ferrite matrix were not evident in field-ion images primarily due to the scavenging of the image gas by the G-phase precipitates and the molybdenum atoms in solution. In the CF 8 aged at 400°C the modulated structures, with a measured periodicity of 7 nm, were clearly visible in field-ion images [Fig. 3(a)]. Field evaporation sequences also revealed that the modulated microstructure was fully interconnected in three dimensions, indicative of phase separation by isotropic spinodal decomposition. The brightly imaging regions were determined to be the iron-rich α phase by selected area analyses. Composition profiles similar to Fig. 2 were also obtained for the aged CF 8. The modulated structures in the aged CF 8 were also

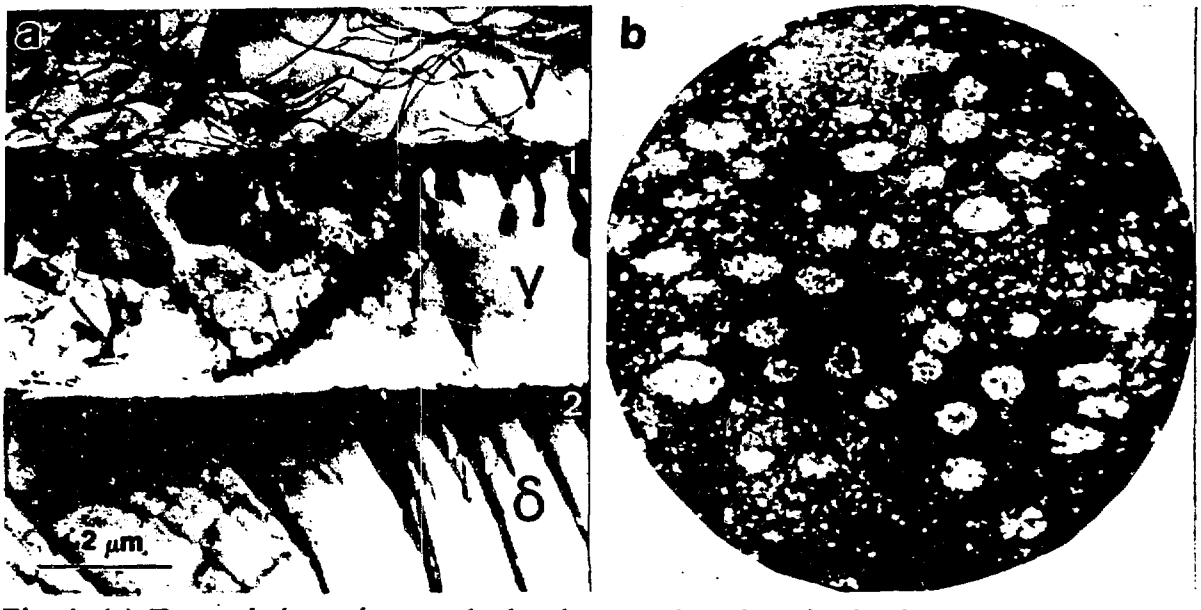

Fig. 1. (a) Transmission micrograph showing γ–δ interface in CF 8 steel aged at 400°C. (b) Field-ion micrograph of the ferrite in the aged CF 8M steel.

Table 2. Compositions of phases in CF 8 aged at 400°C (at.%).

Phase	Cr	Ni	Mn	Mo	Si	Fe
Austenite	20.2	8.4	0.22	0.26	0.99	69.9
Ferrite	28.6	3.7	0.08	0.36	1.42	65.8
$M_{23}C_6$	76.2	2.7	0.0	1.27	0.20	19.6

Table 3. Composition of the G-phase precipitates (at.%).

Element	Si	Cr	Fe+Mn	Ni	Mo	C
APFIM	27.7	12.0	20.6	24.0	13.0	1.0
AEM	20.9	17.8	10.5	31.1	19.9	*

* not determined

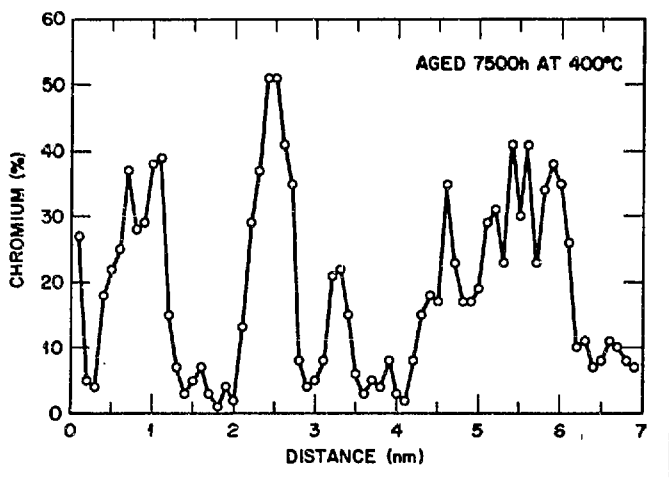

Fig. 2. APFIM composition profile through the ferrite in CF 8M steel aged at 400°C indicates chromium-enriched α' and iron-rich α phases.

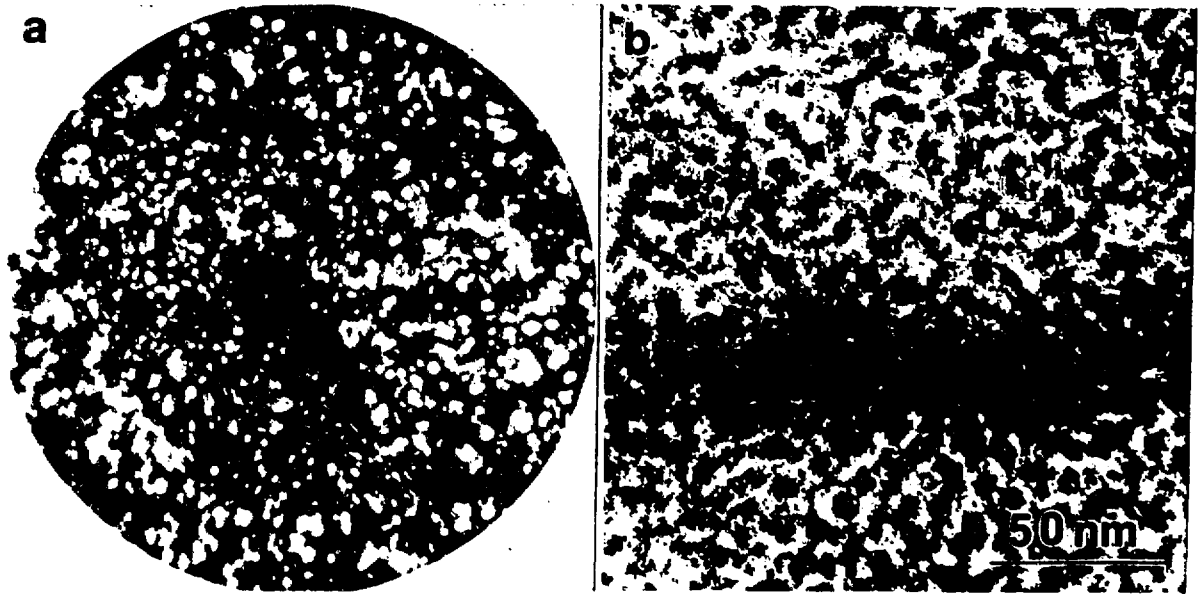

Fig. 3. Modulated structures in the ferrite of CF 8 steel aged at 400°C. (a) Field-ion micrograph showing darkly imaging α' and brightly imaging α phases. (b) Phase-contrast transmission electron micrograph.

visible by phase contrast imaging in the TEM [see Fig. 3(b)]. The modulation periodicities were measured to be 4 and 9 nm in the materials aged at 300 and 400°C, respectively. The precise origin of the TEM contrast is still uncertain and special care was needed to distinguish the effects of oxide films from that of the modulated structure. Composition profiles were not measured by AEM. Although in principle there is adequate spatial resolution with the use of a field emission gun, the analyses require specimens thinner than the modulation periodicity in order to avoid overlap problems.

A dark-field TEM image of the precipitates in the ferrite is shown in Fig. 4(a). All precipitates have the same orientation relationship with the ferrite matrix and the morphological features obtained by FIM are confirmed. X-ray microanalysis of carbon extraction replicas supported on beryllium grids confirmed that the precipitates were alloy silicides. Single particles and aggregated precipitates [Fig. 4(b)] were analyzed. A typical X-ray spectrum is shown in Fig. 4(c) and quantitative results are given in Table 3. Diffraction patterns were obtained from the precipitates plus ferrite matrix. Selected area diffraction (SAD) patterns with beam directions along [001], [011], and [111] are shown in Fig. 4(d-f). All diffraction spots present in SAD patterns were also present in microdiffraction patterns from regions containing a single particle. The patterns are consistent with the precipitates having a fcc structure (Fm3m space group) with a lattice parameter of 1.09 nm, and being oriented cube-on-cube with the ferrite. The lattice parameter of the precipitates is 3.8x that of the ferrite. This mismatch results in splitting of the reflections by double diffraction. Systematic tilting experiments away from zone axes confirmed the double diffraction effects and characteristic relative intensities such as weak 400 and 220 and strong 333 reflections. The exact location of some reflections and the diffuse scattering and streaking are not yet fully understood. Internal faulting may account for the streaking and explain the mottled appearance in dark-field images. Based on the elemental analyses, the diffraction information, and the behavior of similar steels, the precipitates are clearly identified as G-phase.

Distinct bimodal size distributions of G-phase precipitates were observed by TEM in the aged CF 8 steels. The smaller precipitates were randomly distributed in the ferrite matrix, whereas the larger precipitates were associated with dislocations. This is illustrated in Fig. 5 which shows G-phase imaged in dark-field with a 333_g reflection, dislocations imaged under weak-beam dark-field conditions, and a superposition of these images. The finer precipitates were 1.5 and 2 nm in diameter and present at concentrations of $>10^{24}$ and $\sim 10^{21}$ after aging at 300 and 400°C, respectively. In both materials the particles were 4 to 5 times larger on the dislocations than in the matrix.

DISCUSSION

The combination of AEM and APFIM clearly provides a complete characterization of these steels for structure-property correlations. There is a high degree of duplication in the information that each technique provides which is very useful in confirming the correctness of the results. Both techniques were able to resolve the very fine scale α-α' but only APFIM was able to measure the compositions of the two phases. Both techniques were able to detect and analyze the G-phase precipitates. AEM provided additional information on the crystallography, such as the crystal structure and the orientation relationship with the ferrite matrix, that was essential for reliable phase identification. The TEM observations also revealed the bimodal size distributions where the larger precipitates were found to be associated with dislocations. AEM clearly has some advantages for structural characterization at a level intermediate to optical microscopy and nanometer scale microanalysis (e.g. characterization of the ferrite-austenite interface and the determination by X-ray microanalysis of the overall compositions of the various phases) and complements the near-atomic spatial resolution analysis of the APFIM.

Some concerns remain with regard to the absolute accuracy of compositions determined by both techniques for the present application. The accurate measurement of Cr contents by AEM is compromised because of fluorescence by Fe K X-rays. Determination of the overall ferrite matrix composition by APFIM is complicated by biased sampling of the α-α' due to subtle local magnification effects. The G-phase

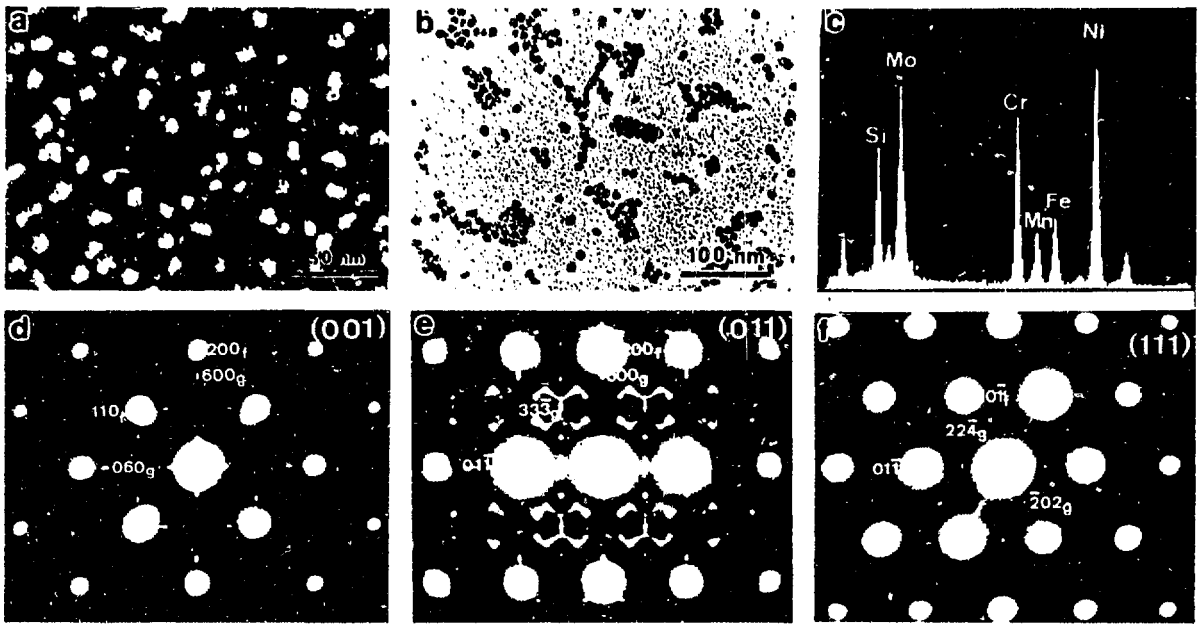

Fig. 4. G-phase precipitates in the ferrite of CF 8M steel aged at 400°C. (a) Dark-field TEM image. (b) Particles on carbon extraction replica. (c) Energy-dispersive X-ray spectrum. (d-f) SAD patterns.

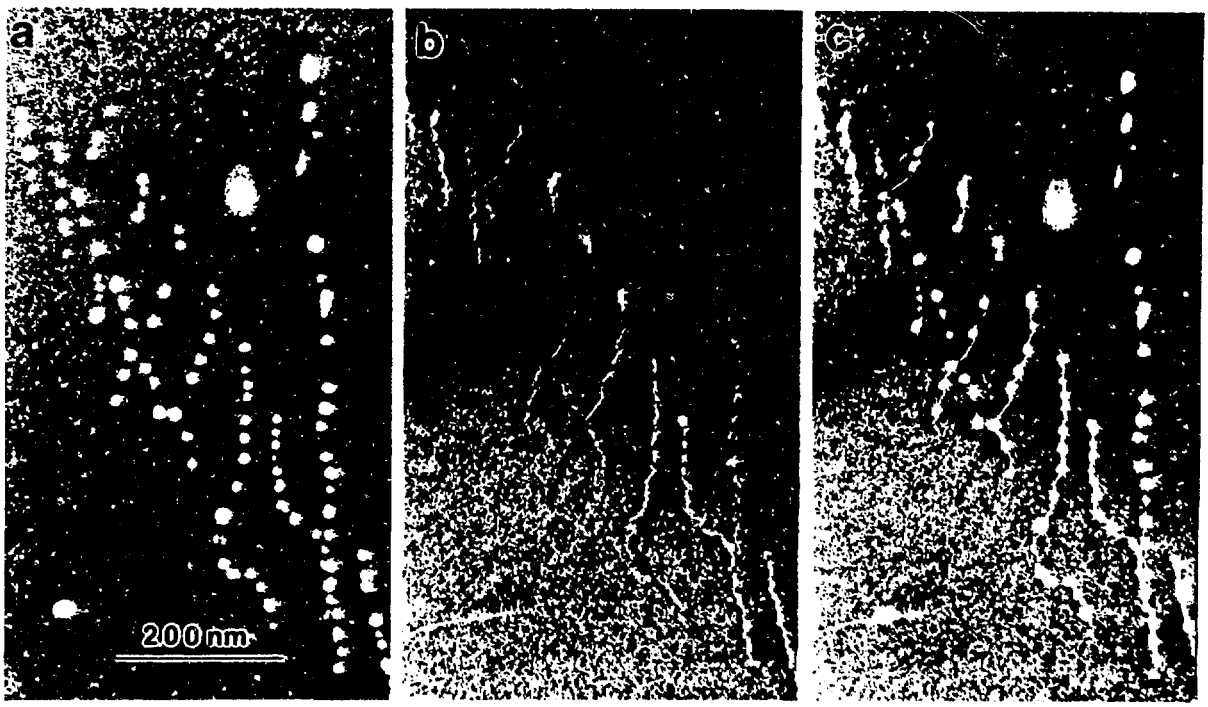

Fig. 5. Transmission electron micrographs of CF 8 steel aged at 400°C showing the coarser G-phase precipitates associated with dislocations. (a) Precipitate-reflection dark-field image. (b) Weak-beam dark-field image showing dislocations. (c) Superposition of (a) and (b).

compositions determined by AEM and APFIM differ significantly. Leaching effects or retained surface films could seriously affect the extracted particles used for the AEM analyses. In addition, the APFIM data were from only the center of the particles (to avoid the matrix) and there is always the possibility of preferential retention or evaporation of particular elements. The above concerns are, however, not major and do not detract from the outstanding characterization capabilities of the combined techniques.

With regard to structure-property correlations, the observed degradation in mechanical properties that occurs during aging is most likely a consequence of the spinodal decomposition in the ferrite. The G-phase precipitation may also contribute, but since this phase was much less prevalent in the CF 8 than in the CF 8M, and the behavior of the two steels is similar, the G-phase is probably not of primary importance. Also, the hardness increases in the CF 8 and CF 8M steels are similar to those previously observed in a spinodally decomposed Fe - 30% Cr alloy that did not contain any G-phase[10].

Finally, careful examination of results from "accelerated" tests at 400°C is required since the reversion of ferrite into austenite with the concurrent precipitation of $M_{23}C_6$ leads to a significantly different microstructure at the ferrite-austenite interface that could radically affect the fracture process and thereby alter the mechanical properties.

ACKNOWLEDGEMENTS

The authors would like to thank Dr. J.A. Spitznagel of Westinghouse R&D Center and Drs. O.K. Chopra and H.M. Chung of Argonne National Laboratory for providing specimen material. This research was sponsored by the Division of Materials Sciences, U.S. Department of Energy under contract DE-AC05-84OR21400 with Martin Marietta Energy Systems, Inc.

REFERENCES

1. S.S. Brenner and M.K. Miller, J. Metals 35 (3), 54-63 (1983).
2. D.B. Williams, Practical Analytical Electron Microscopy in Materials Science, (Philips Electronic Instruments, Inc., Mahwah, NJ, 1984).
3. O.K. Chopra and H.M. Chung, U.S. Nuclear Regulatory Commission/Argonne National Laboratory Report No. NUREG/CR-4503 ANL-86-3, 1986.
4. M.K. Miller, J. Bentley, S.S. Brenner and J.A. Spitznagel, J. de Physique C9, 385-390 (1984).
5. M.K. Miller, J. Bentley, S.S. Brenner and J.A. Spitznagel, in Proc. 43rd Ann. Meeting Electron Microscopy Society of America, ed. G.W. Bailey (San Francisco Press, San Francisco, 1985), p. 326-327.
6. J. Bentley, M.K. Miller, S.S. Brenner and J.A. Spitznagel, in Proc. 43rd Ann. Meeting Electron Microscopy Society of America, ed. G.W. Bailey (San Francisco Press, San Francisco, 1985), p. 328-329.
7. M.K. Miller and J. Bentley, J. de Physique C7, 239-244 (1986).
8. M.K. Miller, J. de Physique, C2, 493 (1986); C2, 499 (1986).
9. N.J. Zaluzec, in Introduction to Analytical Electron Microscopy, eds. J.J. Hren, J.I. Goldstein and D.C. Joy (Plenum Press, New York, 1979) pp. 121-167, Chapter 4.
10. S.S. Brenner, M.K. Miller and W.A. Soffa, Scripta Met. 16, 831 (1982).